Nuclear Inst. and Methods in Physics Research, A 969 (2020) 164064

Contents lists available at ScienceDirect

Nuclear Inst. and Methods in Physics Research, A

journal homepage: www.elsevier.com/locate/nima

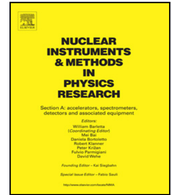

Low-energy proton-induced single event effect in NAND flash memories

Cong Peng [a,c], Wei Chen [a,b], Yinhong Luo [b,*], Fengqi Zhang [b], Xiaobin Tang [a,c,*], Zibo Wang [a,c], Lili Ding [b], Xiaoqiang Guo [b]

[a] *Department of Nuclear Science and Technology, Nanjing University of Aeronautics and Astronautics, Nanjing 210106, China*
[b] *State Key Laboratory of Intense Pulsed Radiation Simulation and Effect, Northwest Institute of Nuclear Technology, Xi'an 710024, China*
[c] *Key Laboratory of Nuclear Technology Application and Radiation Protection in Astronautics, Ministry of Industry and Information Technology, Nanjing University of Aeronautics and Astronautics, Nanjing 210106, China*

ARTICLE INFO

Keywords:
Flash memory
Low-energy proton
Single event effect
Cumulative dose

ABSTRACT

In this paper, the low-energy proton-induced single event effect sensitivity of multiple feature size NAND flash memories has been investigated. Under 0.41 MeV proton, the single event effect cross-section peak appeared in 25 nm and 16 nm flash devices. SRIM simulation revealed the primary reason of this phenomenon. Single event upsets caused by direct ionization of low-energy proton could be several orders of magnitude higher than those caused by high-energy proton nuclear reactions. Moreover, the influence of cumulative dose on the single event effect sensitivity of flash device was investigated. As the cumulative dose increased, the single event upset cross-section was increased considerably. This phenomenon appears due to the threshold voltage shift induced by the combination of the proton and the cumulative dose.

1. Introduction

NAND flash memories have many advantages such as high density, low power consumption, and low cost. They have been widely used in the commercial non-volatile storage market. NAND flash memories manufactured through the floating gate (FG) technology, they can be classified into single-level cell (SLC) and multilevel cell (MLC). MLC further increases storage density by increasing its complexity but sacrificing its reliability. Advanced NAND flash memories have been used in many space applications [1–3].

Unfortunately, the single event effect (SEE) caused by charged particles in the space radiation environment is a severe challenge for the potential space applications of NAND flash memories. Particle irradiation reduces the conductivity of FG tunnel oxide layers and causes to FG charge leakage. Then, the reliability of NAND flash memories is reduced. With the scaling of the FG technology, the linear energy transfer (LET) threshold of SEE is diminished, and the SEE sensitivity of the device is enhanced greatly [4].

The heavy-ion induced SEE of flash memories has been extensively studied [5–11]. The SEEs on the flash memories with multiple feature sizes under heavy ion irradiation were described, and the influences of technology scaling on the LET threshold and saturated cross-section were discussed. The effects of test patterns and ion incidence angles on SEE were also discussed [5–8]. In real space applications, flash devices can accumulate a part of doses, which will affect the SEE cross-section. The heavy-ion induced SEE sensitivity of flash devices with different cumulative doses was studied, and the physical mechanism of SEE sensitivity change was explained [9–11].

Given that the LET value of the proton is small, proton is generally considered incapable of depositing sufficient energy by direct ionization to produce SEE. Rodbell found that low-energy proton direct ionization can lead to single event upset (SEU) on static random access memory [12]. Since then, low-energy proton SEE has attracted wide attention in the field. As feature size decreases, low-energy proton direct ionization can cause a large number of upsets in flash devices. The low-energy proton-induced SEE of advanced flash memories was reported [13]. There are a large number of protons in the space radiation environment. When the protons pass through the spacecraft overlayers, protons deposit most of their energy and stop in the device, which may produce a large number of single event upsets [14]. Ignoring low-energy protons may result in the severe underestimation of the on-orbit error rates of devices. The study on low-energy proton-induced SEE of advanced flash devices are limited, and relevant experimental and theoretical mechanisms need to be supplemented and improved. The sensitivity of flash devices to low-energy proton SEE must be evaluated for their space application.

This work aims to study the low-energy proton-induced SEE sensitivity differences in flash devices of multiple feature sizes down to 16 nm. The paper is organized in the following way. First, the features of devices under test (DUTs) and the experimental details are presented.

* Corresponding authors.
E-mail addresses: luoyinhong@nint.ac.cn (Y. Luo), tangxiaobin@nuaa.edu.cn (X. Tang).

https://doi.org/10.1016/j.nima.2020.164064
Received 31 December 2019; Received in revised form 12 March 2020; Accepted 28 April 2020
Available online 30 April 2020
0168-9002/© 2020 Published by Elsevier B.V.

Table 1
Parameter information of micron NAND flash memories used in the test.

Part number	Date code	Feature size (nm)	Capacity (Gb)	Standard voltage (V)
29F1G08AAC	0940 1–2	120	1	3.3
29F4G08AAC	1010 1–2	72	4	3.3
29F8G08AAA	0918 1–2	51	8	3.3
29F32G08ABAAA	1329 2–2	25	32	3.3
29F32G08CBACA (MLC)	1244-2–7	25	32	3.3
29F64G08CBEFB (MLC)	1538 2–2	16	64	3.3

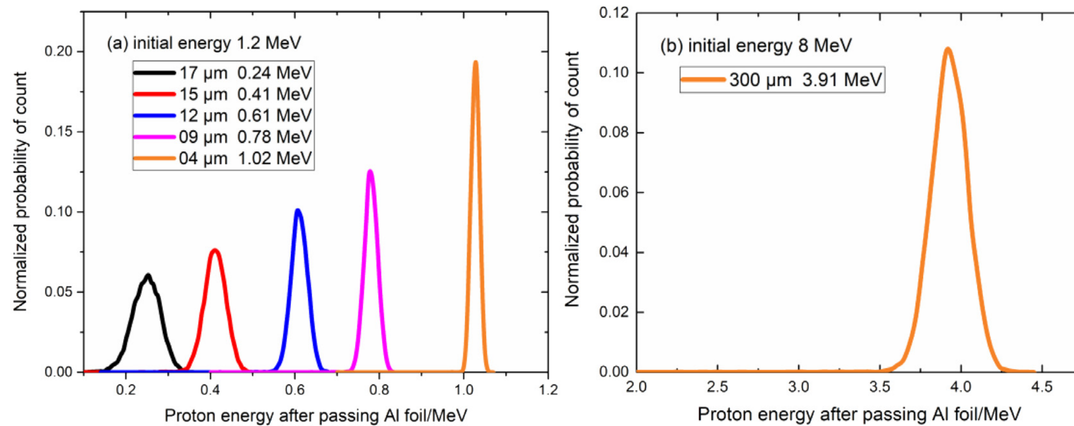

Fig. 1. Energy spectral distribution of multiple initial energy protons after passing through aluminum foils with different thicknesses, (a) initial energy 1.2 MeV; (b) initial energy 8 MeV.

The test results on FG errors induced by low-energy protons are described. Then, the transport of protons in the device is simulated by the SRIM program, and the physical mechanism of low-energy proton-induced SEE is analyzed. Finally, the effect of cumulative dose on the SEE of low-energy protons is explored, and the results are discussed.

2. Device details and experimental setup

In this work, NAND flash memories of multiple feature sizes with SLC and MLC architecture were used. All DUTs were manufactured by Micron Technology. Information on DUTs is shown in Table 1.

The SEE experiments under 50 and 90 MeV protons were performed on the 100 MeV proton cyclotron at the China Institute of Atomic Energy in previous work. A low-energy proton irradiation test was conducted at the EN tandem accelerator of the Institute of Heavy Ion Physics, Peking University. The EN tandem accelerator provided 1.2–10 MeV protons, the vacuum was 10^{-3} Pa in the chamber and the test at room temperature. According to the requirements of the test, multiple proton energies were selected, which were shown in Table 2. LETs corresponding to proton energy calculated using SRIM was also listed. Given that the minimum proton energy of the EN tandem accelerator was 1.2 MeV, aluminum foils were used to obtain the protons with energy lower than 1.2 MeV. Aluminum foils with different thicknesses were selected to degrade proton energy (Table 2). To save experimental time, 3.9 MeV protons were also obtained by using aluminum foils to degrade 8 MeV protons. SRIM was used to calculate the proton energy spectrum distribution after 1.2 and 8 MeV protons passing through different thicknesses aluminum foils, as shown in Fig. 1.

Given that low-energy protons have short ranges, the experiments were performed in vacuum environment. The DUTs were exposed to the proton beam and plastic packaging was removed by etching the DUTs. The SEE sensitivity of the device FG array was examined with normal proton incidence on all unpowered devices. The DUTs were placed on the irradiation board and were programmed to checkerboard “55” before the test. All the test samples were detected immediately after proton irradiation, and the number and address locations of FG upsets were recorded.

Table 2
Average proton energy and LET for various aluminum foil degrader settings.

Initial energy (MeV)	The thickness of Al foil (μm)	Average energy (MeV)	LET (MeV cm^2/mg)	Range in Si (μm)
8	0	8	0.041	482.01
8	300	3.91	0.070	142.82
1.2	0	1.2	0.157	21.48
1.2	4	1.02	0.174	16.82
1.2	9	0.78	0.202	11.32
1.2	12	0.61	0.230	7.93
1.2	15	0.41	0.283	4.56
1.2	17	0.24	0.364	2.28

Owing to the time limitation of the proton beam, the influence of cumulative dose on low-proton SEE sensitivity was only explored in 32 G SLC devices. During the experiment, 1.2 MeV protons were used to accumulate different total doses in devices. Then, the unpowered device was irradiated under low-energy proton, and the SEE cross-sections with different cumulative doses were tested. All samples were detected after irradiation in a few minutes, and the annealing effect was not considered. In order to have more visibility on low-proton induced SEE, Error-correcting code (ECC) was not applied in the test devices.

3. Results and discussion

3.1. Low-energy proton-induced single event upsets

The low-energy proton SEE experiment was performed on SLC and MLC flash devices and a self-developed flash memory test system was used. The data were detected after irradiation of 4×10^8–1×10^9 p/cm^2 protons. A few inherent errors in MLC devices were deducted when their SEU cross-sections were calculated.

Results showed that no error was detected in the 1, 4, and 8 G samples under proton irradiation when the energy of protons was lower than 1.2 MeV. For these flash devices whose feature sizes larger than 25 nm, no SEU was observed due to the high LET threshold of SEE in the devices.

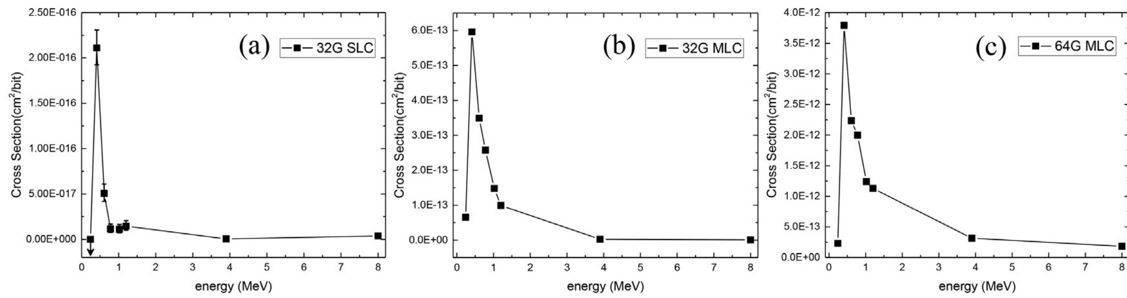

Fig. 2. SEU cross-section of DUTs vs. energy under low-proton irradiation. The downward arrow indicates that no SEU was detected. (a) 32 G SLC; (b) 32 G MLC; (c) 64 G MLC.

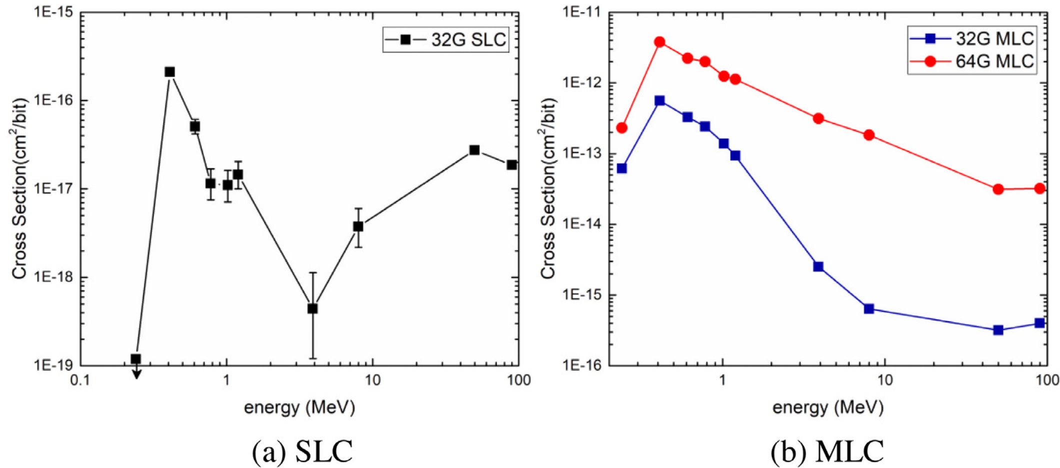

Fig. 3. Proton SEU cross-section vs. proton energy for the SLC and MLC devices. The downward arrow indicates that no SEU was detected.

However, a large number of SEUs were produced in the 32 G SLC, 32 G MLC, and 64 G MLC devices under proton irradiation, the feature sizes of devices were 25 nm and 16 nm. Fig. 2 shows the variation in SEU cross-section with proton energy. The error bars are ~2 sigma (95%) and result from Poisson statistics. The SEU cross-section peak appeared in all devices under 0.41 MeV proton irradiation. For the 32 G SLC device, the SEU cross-section was 2.11×10^{-16} cm^2/bit under 0.41 MeV proton irradiation and 3.75×10^{-18} cm^2/bit under 8 MeV proton irradiation. The SEU cross-section at the peak was approximately two orders of magnitude higher than the cross-section under 8 MeV proton irradiation. The 25 nm and 16 nm flash devices were highly sensitive to low-energy protons. Low-energy proton irradiation can cause many SEUs in devices.

The proton-induced SEU cross-section curves from low-energy to high-energy were drawn to compare with those of SEU caused by high energy protons. Fig. 3 shows the proton SEU cross-section as a function of proton energy for the SLC and MLC devices with multiple feature sizes, including the SEE test results of the high-energy proton (50 and 90 MeV) at the China Institute of Atomic Energy [15]. MLC samples had a higher SEE cross-section than SLC samples at the same feature size due to the smaller error margins between adjacent levels. Under 0.41 MeV proton irradiation, the SEE cross-section at the peak of the 16 nm device was approximately an order of magnitude higher than that of the 25 nm device. Compared with the 25 nm device, the charges stored in the FG cell of the 16 nm device was less. Owing to the critical charge required for SEE and error margins between adjacent levels reduced, the SEE sensitivity of the device was enhanced. In addition, the 16 nm device had a larger capacity than the 25 nm device, and the FG cells had a higher density and smaller clearance. Proton irradiation produces ionization in a particular track area of the device. There were more substantial cells in the track area due to the smaller feature size, and the probability of device producing multiple bit upsets increased. Finally, as the feature size was scaled down, the devices became more sensitive. As proton energy increased to the high-energy region, the SEE cross-section of the device gradually became saturated. Compared with the cross-section peak at low-energy proton, the cross-section at high-energy proton was substantially lower.

Longitudinal anatomy analysis of the device was performed to study the effect of low-energy proton on the device. The hierarchical structure, elemental composition, location depth, and other information of the device were obtained, as shown in Fig. 4. The polymetallic layer changes the energy of the incident protons, thereby reducing the energy and broadening the energy spectrum. The SRIM program was used to simulate the transport of protons in an approximate cell structure, so as to correctly evaluate the energy loss in the multi-metal layer above the FG electrode.

Fig. 5 shows the LET value distribution of protons in Si versus energy. When proton energy was close to 55 keV, the LET reached the highest value (Bragg peak). Fig. 6 shows that the energy spectrum distribution and LET value varied with incident depth after protons passing through the polymetallic layer. For these devices, the 0.24 MeV proton had lost all energy before it penetrated the polymetallic layer; hence, the energy spectrum distribution curve of 0.24 MeV proton incident could not be formed. In Fig. 6b, d, and f, the black vertical line is the sensitive area, the left side of the black vertical line was the polymetallic layer area, and the right side was the Si substrate. Protons deposited a certain amount of energy in the FG sensitive area by direct ionization. The main effect of protons was to discharge the FG cells, which can lead to the SEU of the device. After the proton penetrates the polymetallic layer, the higher the LET value of the proton reaches the sensitive area, the more energy is deposited, and the larger the SEE cross-section of the device.

When the energy was 0.41 MeV, the end of the proton range was mainly concentrated in the device sensitive area. After passing through the polymetallic layer of the device, the proton energy was mainly distributed between 0.01 and 0.1 MeV. The energy was located near

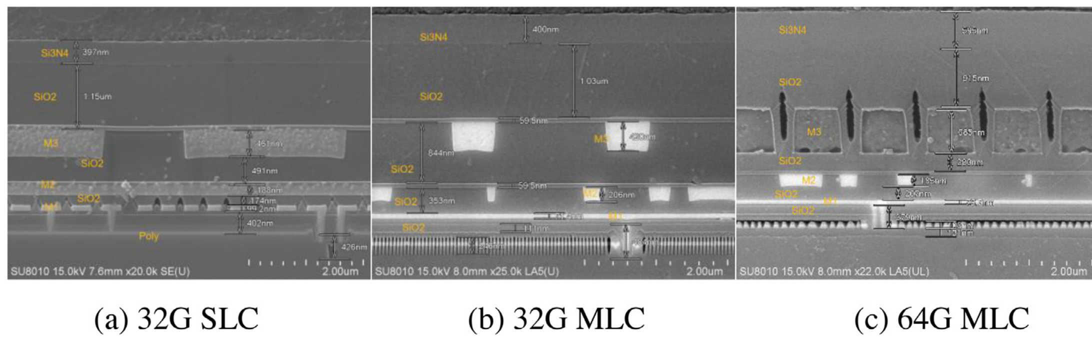

Fig. 4. Longitudinal sections of several flash devices.

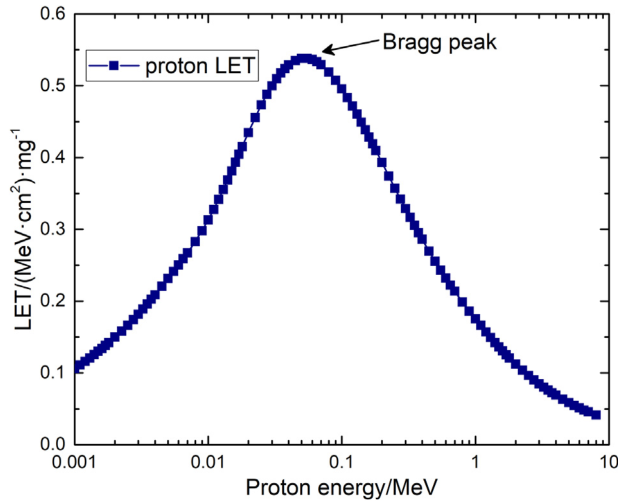

Fig. 5. Proton LET value distribution with the energy in Si.

the Bragg peak, and its LET reached the maximum value. The sufficient energy could be deposited in the FG sensitive region by protons direct ionization, which can generate a large number of SEUs. When the energy was lower than 0.41 MeV, a large number of protons could not effectively deposit energy in the FG sensitive area due to its limited range. It is noted that the 0.24 MeV proton was obtained by degrading 1.2 MeV protons through aluminum foil, and the energy spectrum was broadened (Fig. 1a). The high-energy proton in the energy spectrum can also deposit a part of the energy into the sensitive area to generate SEUs. However, owing to its low flux, the SEU cross-section caused by 0.24 MeV protons was lower considerably than that caused by 0.41 MeV protons. When the energy reached 0.61 MeV, the protons with a greater range directly passed through the sensitive region of the FG cell. After the protons passed through the polymetallic layer, the energy spectrum was broadened. Some protons had lower energy in the energy spectrum, and the corresponding LET value exceeded the SEU threshold of the device, leading to SEU in the device. As the energy increased, the LET value of proton in the sensitive area and the SEU cross-section are both decreased.

When the energy of the protons less than 1.2 MeV, the SEU of the device was caused by low-energy proton direct ionization. When the energy exceeded 3 MeV, SEU was mainly caused by secondary particles generated by the collision of protons with the FG material atomic nucleus. Owing to the direct ionization LET value and the nuclear reaction probability were small, the SEU cross-section caused by more than 3 MeV protons is lower than that caused by low-energy protons. Thereafter, as the proton energy increased, the cross-section of the high-energy proton nuclear reaction was getting stable, and the SEU cross-section of the device was gradually saturated.

3.2. Influence of cumulative dose on single event effect

After a specific total dose was accumulated (10, and 20 krad in Si) by 1.2 MeV protons, the device was reprogrammed to checkerboard "55". The low-energy proton SEE test was performed after ensuring that the device had no hard function error. The test was not performed at all energies due to the time limitation of the proton beam. The relationship between proton irradiation dose, proton fluence (Φ) and LET can be expressed as

$$\mathrm{TID\,(rad\,(\,Si))} = 1.6 \times 10^{-5} \times \Phi(\mathrm{cm}^{-2}) \times \mathrm{LET}(\mathrm{MeV} \cdot \mathrm{cm}^2/\mathrm{mg}) \quad (1)$$

Fig. 7 shows the device SEU cross-section with different doses as a function of proton energy. Obviously, the higher the dose accumulated before the SEE test, the higher the SEU cross-section of the device would be. When the dose was 10 krad (Si) and the proton energy were 0.41, 0.61, and 0.78 MeV, the enhancement factors of the device SEU cross-section were 1.42, 1.42, and 2.23, respectively. When the dose was 20 krad (Si) and the proton energy were 0.41, 0.61, and 0.78 MeV, the enhancement factors of the device SEU cross-section were 2.53, 2.70, and 5.34, respectively.

After a specific dose was accumulated, a large number of electron–hole pairs were generated in the tunnel oxide layer of the FG cell, and some electron–hole pairs were recombined immediately. The electrons in the unrecombined electron–hole pair quickly escaped from the oxide layer, and the holes slowly drifted toward the FG and neutralized with the FG electrons [16]. In addition, when FG electrons gain sufficient energy from impinging radiation, some electron emissions jump over the tunnel oxide barrier [17]. Charge neutralization and electron emission can reduce the number of electrons stored in the FG. Moreover, some defects are produced by irradiation in an FG cell tunnel oxide, and the defects will trap the charge generated by irradiation [18,19]. The mechanisms, such as charge trapping, electron emission, and charge neutralization, are identified as the cause of the total dose effect (TID). However, the device was reprogrammed after accumulating a given dose, and the FG charges were replenished. Consequently, electron emission and charge neutralization by TID were not considered in the subsequent SEE tests. The charge trapping shifts the threshold voltage V_{th} of the FG cell to the left. TID usually deposits a uniform dose in all cells of the device.

The device was performed SEE tests after accumulating a given dose. When the device is irradiated, the transient carrier current of tunnel oxide, the transient conductive path, and electron emission are formed by particle incidence in the FG cell [20,21]. These factors lead to instantaneous leakage loss of FG charges, which can cause a remarkable shift of the threshold voltage V_{th}. The mechanisms, such as transient carrier current and transient conductive path, are identified as the cause of the SEE [8,22]. If the threshold voltage V_{th} of the FG cell is lower than the read voltage, the device will generate data upsets.

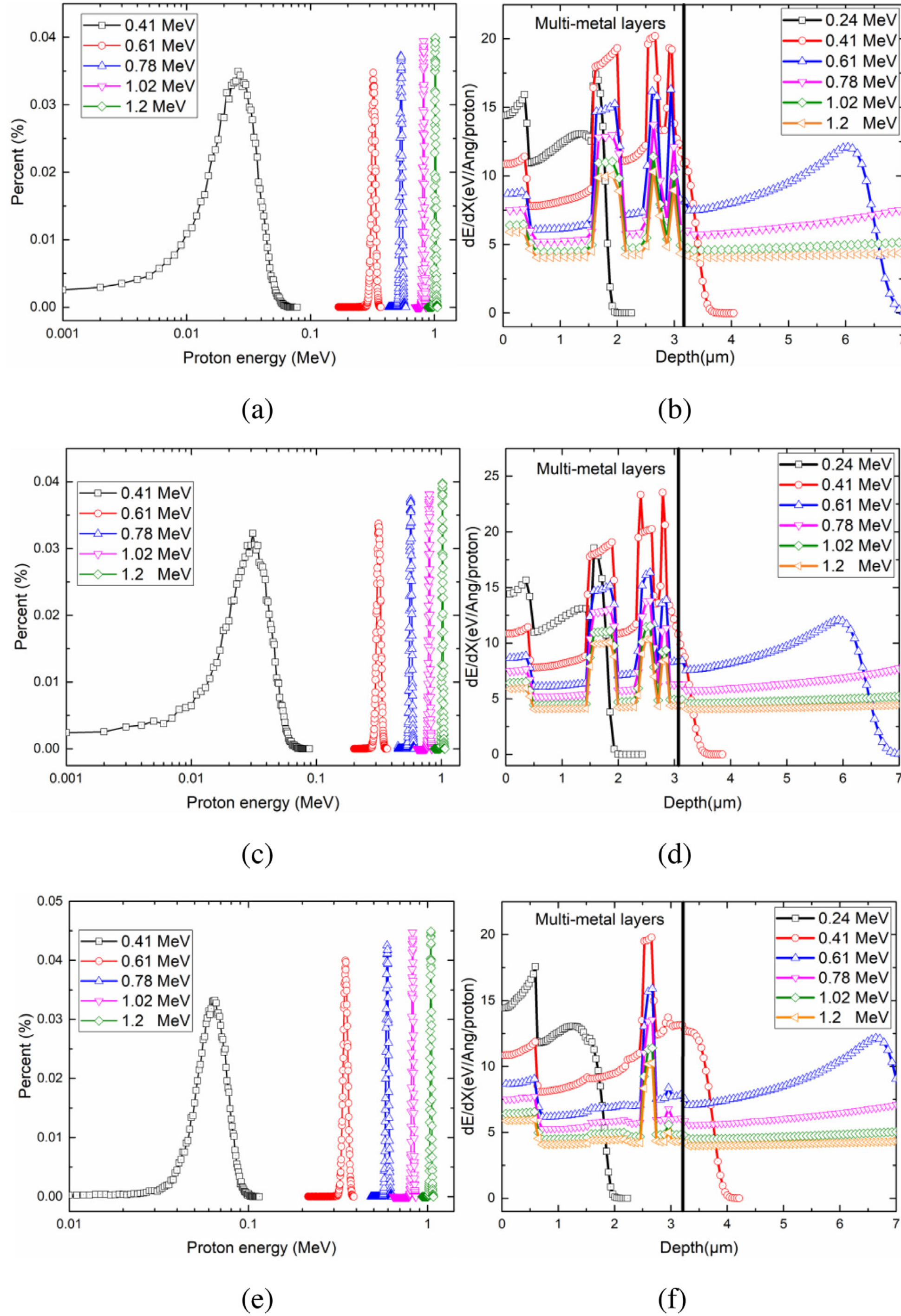

Fig. 6. Energy spectrum distribution and the LET value vary with incident depth after protons passing through the polymetallic layer, (a) energy spectrum of 32 G SLC; (b) LET vs. proton incident depth in 32 G SLC; (c) energy spectrum of 32 G MLC; (d) LET vs. proton incident depth in 32 G MLC; (e) energy spectrum of 64 G MLC; (f) LET vs. proton incident depth in 64 G MLC.

Fig. 8a is the schematic diagram of charge trapping, charge neutralization and transient leakage current inside the programmed FG cell during irradiation. Fig. 8b shows the shift of the FG cell threshold voltage V_{th} by low-energy proton irradiation after accumulated different doses. The threshold voltage V_{th} of all FG cells shifted to the left as a whole by the cumulative dose. The more dose was accumulated, the more considerable the threshold voltage shift. However, only a portion of the FG cell threshold voltage V_{th} shifted to the left under proton irradiation, forming a threshold voltage tail. The threshold voltage V_{th} shift caused by dose and proton irradiation was cumulatively superposed.

The total threshold voltage shift $\triangle V_{th}$ can be approximately expressed as follows:

$$\triangle V_{th} = \triangle V_{th,TID} + \triangle V_{th,SEE} \tag{2}$$

where $\triangle V_{th,TID}$ is the threshold voltage V_{th} shift caused by TID, and $\triangle V_{th,SEE}$ is the threshold voltage shift caused by proton irradiation. The total number of errors [9] is obtained from the following formula:

$$\#error = \int_{-\infty}^{V_{read}} V_{th,P}(V)dV + \int_{V_{read}}^{V_{read}+\triangle V_{th,TID}} V_{th,P}(V)dV \tag{3}$$

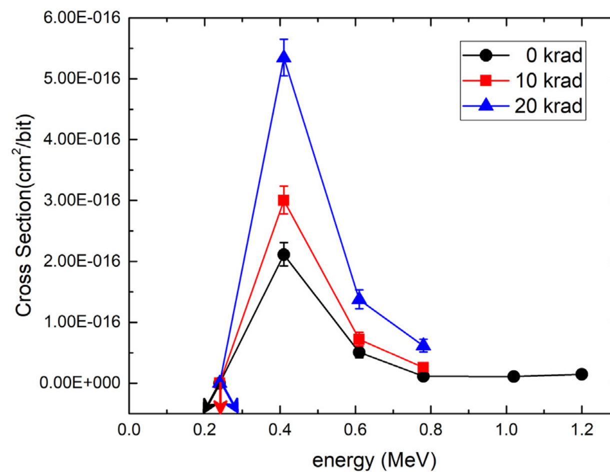

Fig. 7. SEU cross-section with different doses vs. proton energy. The downward arrow indicates that no SEU was detected.

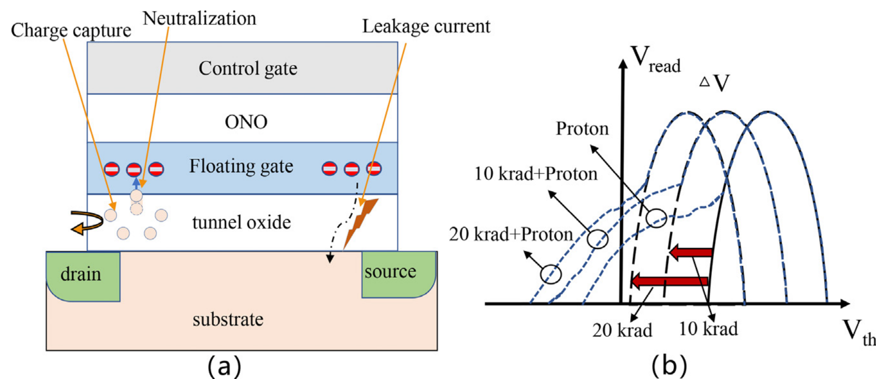

Fig. 8. Dose and proton induced FG error. (a) effect mechanisms; (b) shift of threshold voltage V_{th}.

where $V_{th,P}(V)$ represents the threshold voltage V_{th} distribution before irradiation. Two items are on the right side of formula (3); the first item I1 is the SEUs caused by proton irradiation and the second item I2 is the SEU increment generated by the irradiation dose. The larger the irradiation dose, the larger the threshold voltage shift $\triangle V_{th,TID}$. Ultimately, the increment I2 of the proton SEU caused by the irradiation dose was also greater. The 20 krad (Si) dose used in the present study represents the typical dose level in aerospace space. The experimental results show that neglecting the influence of dose can severely underestimation of the proton-induced SEU rate.

4. Conclusion

In this study, the SEEs on flash devices with multiple feature sizes were examined using low-energy protons. The experimental results showed that 25 nm and 16 nm NAND flash memory were sensitive to low-energy protons. The SEU caused by low-energy proton direct ionization can be several orders of magnitude higher than that caused by high-energy proton nuclear reactions. Ignoring the effect of low-energy proton may result in underestimation of the device's spatial SEU rate.

Electronic devices are simultaneously affected by multiple irradiance effects in space applications. The influence of cumulative dose on SEE of 25 nm flash device was investigated. The experimental results showed that the cumulative dose could substantially increase low-energy proton-induced SEU cross-section of the 25 nm SLC flash device. As the cumulative dose increased, the SEU cross-section of the device increased considerably. This phenomenon is attributed to the combined shift of FG cell threshold voltage V_{th} caused by the proton and the cumulative dose.

CRediT authorship contribution statement

Cong Peng: Data curation, Writing - original draft. **Wei Chen:** Supervision, Funding acquisition. **Yinhong Luo:** Formal analysis. **Fengqi Zhang:** Validation. **Xiaobin Tang:** Writing - review & editing. **Zibo Wang:** Investigation. **Lili Ding:** Methodology. **Xiaoqiang Guo:** Resources.

Declaration of competing interest

The authors declare that they have no known competing financial interests or personal relationships that could have appeared to influence the work reported in this paper.

Acknowledgments

This work was supported by the Major Program of the National Natural Science Foundation of China (Grant Nos. 11690043, 11690040); the National Natural Science Foundation of China (Grant No. 11675076).

References

[1] M. D'Alessio, C. Poivey, D. Walter, K. Gruermann, F. Gliem, H. Schmidt, R.H. Sorensen, A. Keating, N. Fleurinck, K. Puimege, NAND flash memory in-flight data from PROBA-II spacecraft, in: 14th European Conference on Radiation and its Effects on Components and Systems, Oxford, UK, 2013.

[2] M. Fabiano, G. Furano, NAND flash storage technology for mission-critical space applications, IEEE Aerosp. Electron. Syst. Mag. 28 (2013) 30–36.

[3] K. Grürmann, M. Herrmann, F. Gliem, H. Schmidt, G. Leibeling, H. Kettunen, V. Ferlet-Cavrois, Heavy ion sensitivity of 16/32-Gbit NAND-Flash and 4-Gbit DDR3 SDRAM, in: IEEE Radiat. Eff. Data Workshop, Tucson, AZ, USA, 2012.

[4] M. Bagatin, S. Gerardin, A. Paccagnella, V. Ferlet-Cavrois, Single and multiple cell upsets in 25-nm NAND flash memories, IEEE Trans. Nucl. Sci. 60 (2013) 2675–2681.

[5] F. Irom, D.N. Nguyen, M.L. Underwood, A. Virtanen, Effects of scaling in SEE and TID response of high density NAND flash memories, IEEE Trans. Nucl. Sci. 57 (2010) 3329–3335.

[6] M. Bagatin, S. Gerardin, A. Paccagnella, A. Visconti, Impact of technology scaling on the heavy-ion upset cross-section of multi-level floating gate cells, IEEE Trans. Nucl. Sci. 58 (2011) 969–974.

[7] D. Chen, E. Wilcox, R.L. Ladbury, H. Kim, A. Phan, C. Seidleck, K.A. LaBel, Heavy ion irradiation fluence dependence for single event upsets in a NAND flash memory, IEEE Trans. Nucl. Sci. 64 (2017) 332–337.

[8] M. Bagatin, S. Gerardin, A. Paccagnella, Space and terrestrial radiation effects in flash memories, Semicond. Sci. Technol. 32 (2017) 033003.

[9] M. Bagatin, S. Gerardin, A. Paccagnella, G. Cellere, A. Visconti, M. Bonanomi, Increase in the heavy-ion upset cross-section of floating gate cells previously exposed to TID, IEEE Trans. Nucl. Sci. 57 (2010) 3407–3413.

[10] S. Gerardin, M. Bagatin, A. Paccagnella, G. Cellere, A. Visconti, M. Bonanomi, Impact of total dose on heavy-ion upsets in floating gate arrays, Microelectron. Reliab. 50 (2010) 1837–1841.

[11] Y. Yin, J. Liu, Q. Ji, P. Zhao, T. Liu, B. Ye, J. Luo, Y. Sun, M. Hou, Influences of total ionizing dose on single event effect sensitivity in floating gate cells, Chin. Phys. B 27 (2018) 086103.

[12] K.P. Rodbell, D.F. Heidel, H.H.K. Tang, M.S. Gordon, P. Oldiges, C.E. Murray, Low-energy proton-induced single event-upsets in 65 nm node, silicon-on-insulator, latches and memory cells, IEEE Trans. Nucl. Sci. 54 (2007) 2474–2479.

[13] M. Bagatin, S. Gerardin, A. Paccagnella, A. Visconti, A. Virtanen, H. Kettunen, A. Costantino, V. Ferlet-Cavrois, A. Zadeh, Single event upsets induced by direct ionization from low-energy protons in floating gate cells, IEEE Trans. Nucl. Sci. 64 (2017) 464–470.

[14] N.A. Dodds, M.J. Martinez, P.E. Dodd, M.R. Shaneyfelt, F.W. Sexton, J.D. Black, D.S. Lee, S.E. Swanson, B.L. Bhuva, K.M. Warren, R.A. Reed, J. Trippe, B.D. Sierawski, R.A. Weller, N. Mahatme, N.J. Gaspard, T. Assis, R. Austin, S.L. Weeden-Wright, L.W. Massengill, G. Swift, M. Wirthlin, M. Cannon, R. Liu, L. Chen, A.T. Kelly, P.W. Marshall, M. Trinczek, E.W. Blackmore, S.J. Wen, R. Wong, B. Narasimham, J.A. Pellish, H. Puchner, The contribution of low-energy protons to the total on-orbit SEU rate, IEEE Trans. Nucl. Sci. 62 (2015) 2440–2451.

[15] C. Peng, W. Chen, Y. Luo, F. Zhang, X. Tang, X. Guo, J. Sheng, L. Ding, Z. Wang, Proton-induced single-event effect and influence of annealing on multiple feature size NAND flash memory, Japan. J. Appl. Phys. 58 (2019) 126002.

[16] G. Cellere, A. Paccagnella, S. Lora, A. Pozza, A. Scarpa, Charge loss after ^{60}Co irradiation on Flash arrays, IEEE Trans. Nucl. Sci. 51 (2004) 2912–2916.

[17] G. Cellere, A. Paccagnella, A. Visconti, M. Bonanomi, S. Beltrami, J.R. Schwank, M.R. Shaneyfelt, P. Paillet, Total ionizing dose effects in NOR and NAND flash memories, IEEE Trans. Nucl. Sci. 54 (2007) 1066–1070.

[18] M. Bagatin, S. Gerardin, G. Cellere, A. Paccagnella, A. Visconti, S. Beltrami, R. Harboe-Sorensen, A. Virtanen, Key contributions to the cross-section of NAND flash memories irradiated with heavy ions, IEEE Trans. Nucl. Sci. 55 (2008) 3302–3308.

[19] Y. Yin, J. Liu, Y. Sun, M. Hou, T. Liu, B. Ye, Q. Ji, J. Luo, P. Zhao, Anomalous annealing of floating gate errors due to heavy ion irradiation, Nucl. Instrum. Methods Phys. Res. B 418 (2018) 80–86.

[20] N.Z. Butt, M. Alam, Modeling single event upsets in Floating Gate memory cells, in: IEEE International Reliability Physics Symposium, Phoenix, AZ, USA, 2008.

[21] G. Cellere, A. Paccagnella, A. Visconti, M. Bonanomi, A. Candelori, Transient conductive path induced by a Single ion in 10 nm SiO_2 Layers, IEEE Trans. Nucl. Sci. 51 (2004) 3304–3311.

[22] S. Gerardin, M. Bagatin, A. Paccagnella, K. Grurmann, F. Gliem, T.R. Oldham, F. Irom, D.N. Nguyen, Radiation effects in flash memories, IEEE Trans. Nucl. Sci. 60 (2013) 1953–1969.